Available online at www.sciencedirect.com

ScienceDirect

Ceramics International 40 (2014) 2869–2876

CERAMICS INTERNATIONAL

www.elsevier.com/locate/ceramint

Microwave synthesis and sintering of forsterite nanopowder produced by high energy ball milling

H. Barzegar Bafrooei*, T. Ebadzadeh, H. Majidian

Ceramic Division, Materials and Energy Research Center, P.O. Box 14155-4777, Karaj, Alborz, Iran

Received 30 September 2013; accepted 6 October 2013
Available online 18 October 2013

Abstract

This paper reports the development of a new process for the synthesis and sintering of forsterite nanopowder via microwave-assisted high energy ball milling of a powder mixture containing silica gel and $Mg(OH)_2$. X-ray diffraction (XRD), FTIR spectrometer, BET, scanning electron microscopy (SEM) and Transmission electron microscopy (TEM) techniques were utilized to characterize the as-milled and annealed samples. X-ray diffraction results showed that highly ordered forsterite can be obtained through the calcination of the as-milled powder over 900 °C. In addition, SEM and TEM observations of the synthesized powders showed that the particle size of the powder lies in the nanometer range, also being compared with the BET results (about 45 to 64.5 nm). Microwave sintering (MS) of the forsterite nanopowder produced with high energy ball milling and subsequent microwave heating resulted in remarkable enhancement in densification in comparison with conventional sintering (CS) at lower temperatures.

Keywords: A. Sintering; Microwave heating; Synthesis; Forsterite; High energy ball milling

1. Introduction

Modern technologies constantly require materials with special properties to achieve breathtaking innovations. This, in turn, requires constant improving of scientific and technological fabrication as well as working procedures. Nanocrystalline materials are single-phase or multi-phase materials, whose crystal size is in the order of a few (typically 1–100) nanometers at least in one dimension. Because of the extremely small size of the grains, a large fraction of the atoms in these materials is located in the grain boundaries and thus the material exhibits enhanced combinations of physical, mechanical, and magnetic properties (compared to material with a more conventional grain size, i.e., >1 μm). Therefore, nanocrystalline materials show increased strength, high hardness, extremely high diffusion rates, and consequently reduced sintering times for powder compaction [1]. Forsterite is a crystalline magnesium silicate with chemical formula Mg_2SiO_4, named after the German naturalist Johann Forster. Forsterite (Mg_2SiO_4) is an important material of olivine family of crystals in the magnesia–silica system with orthorhombic structure [2]. The extremely low electrical conductivity of forsterite makes it an ideal material for tunable laser [3–5]. Moreover, it shows good refractoriness with high melting point (1890 °C), low thermal expansion, good chemical stability and excellent insulation properties even at high temperatures [6–8]. The manufacturers of the SOFC (solid oxide fuel cells) find forsterite interesting due to its linear thermal expansion coefficient perfectly matching the other cell components and a very high stability in fuel cell environments [9]. In the recent years, much attention has been paid to the development of microwave telecommunication technologies because of the increased requirements for microwave applications. Among these materials, forsterite Mg_2SiO_4 has attracted a great deal of attention due to its low dielectric constant and loss tangent [10,11]. Furthermore, forsterite bioceramic possesses good biocompatibility and mechanical properties and might be suitable for hard tissue repair [12–14]. Various techniques including the heating of mixed powders prepared by the alkoxy method [15], the polymer matrix method [16], the citrate–nitrate route [17], the sol–gel method [18–20], the

*Corresponding author. Tel.: +98 2636204130; fax: +98 2636280030.
E-mail address: hadi.merc@gmail.com (H. Barzegar Bafrooei).

0272-8842/$ - see front matter © 2013 Elsevier Ltd and Techna Group S.r.l. All rights reserved.
http://dx.doi.org/10.1016/j.ceramint.2013.10.025

combustion method [21] and high energy ball milling have been used to synthesize forsterite [22–24]. It is been recently found that microwave energy can be used to synthesize ceramic powders where reactions of component oxides at elevated temperatures are involved [25]. Microwave synthesis of materials is fundamentally different from the conventional synthesis in terms of its heating mechanism. In the microwave furnace, the interaction of microwaves with the material generates heat within the sample volume [26]. Moreover, microwave energy heats the material on a molecular level which leads to uniform heating, whereas conventional heating systems would heat the sample up from the surface towards the interior zones, giving rise to steep thermal gradients [27]. The microwave assisted preparation of nanopowders is a new method that includes the hydrothermal, hydrolysis and co-precipitation methods [28–30]. In this paper, a novel approach which is the combination of ball milling and microwave heating for the synthesis and sintering of forsterite has been developed.

2. Experimental

2.1. Materials

Silica gel and magnesium hydroxide ($Mg(OH)_2$) were used as the starting materials for the synthesis of forsterite. Figs. 1 and 2(a, b) show the XRD and morphology of the initial powder agglomerates. The XRD pattern of raw materials was characterized according to those of silica gel (amorphous pattern) and $Mg(OH)_2$ (XRD JCPDS data reference code 007-0239). The $Mg(OH)_2$ powder has an angular shape with a mean agglomerate diameter of about 5 μm. Silica gel powder has a spherical shape with a mean agglomerate size of about 1–2 μm. The agglomerate size of powders was determined using scanning electron microscope (SEM). Also several micrographs were used for agglomerate size measurement and the average value was reported.

2.2. Experimental procedure

The milling experiment was carried out with Planetary Mill. A zirconia vial with diameter of 80 mm and 25 zirconia balls with diameter of 15 mm were used as the milling medium. The required amount of powder mixture for 15:1 ball to powder mass ratio (BPMR) was taken from the homogeneous mixture of powders and placed in the bowl for ball milling. The raw materials were milled in air at room temperature for 0.25, 5, 10, 20, 30 and 40 h, respectively. The rotation speed of the disk was 270 rpm and that of the vials was 675 rpm. The milled powders were calcined at 500–1200 °C by microwave heating in the air. Powders pre-pressed up to ~49.5% of the theoretical density were sintered in two different ways: (i) conventional sintering (CS) via continuous heating up to different temperature (1150–1350 °C) with a heating rate of 10 °C/min, (ii) microwave sintering (MS) through heating up to the same temperature with conventional sintering in a 1.1 kW, 2.45 GHz multimode microwave cavity (Bosch, Germany).

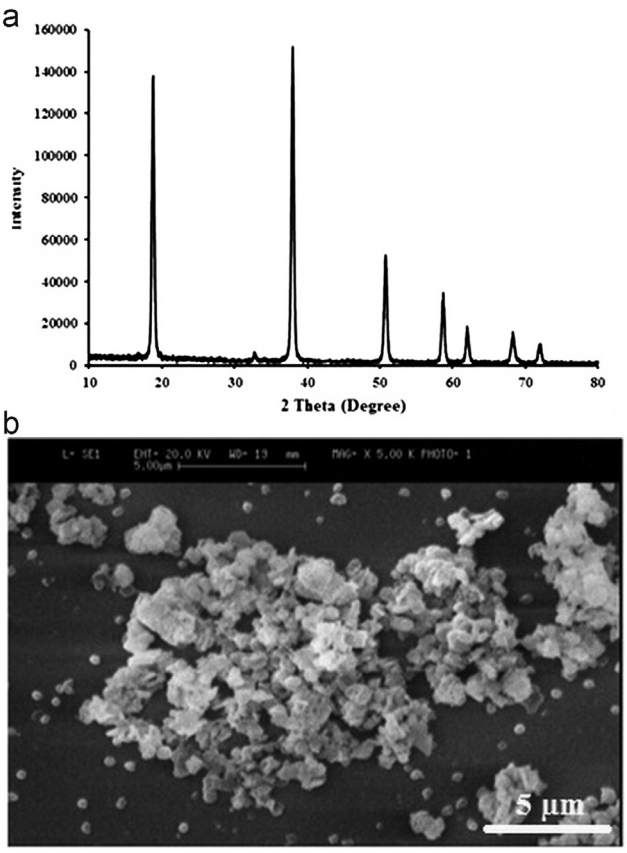

Fig. 1. (a) XRD and (b) SEM $Mg(OH)_2$ powder before high energy ball milling.

2.3. Characterization

The structural properties of the samples were investigated by X-ray diffraction (Simens D-500 system) technique using a CuKα monochromatized radiation source and Ni filter in the range 2θ=10–80. The morphology, microstructure and the particle size of the high energy ball milled powders and sintered samples were examined by a Philips scanning electron microscope (SEM) operating at 20 kV and Transmission electron microscopy (TEM, TecnaiF20, Phillip, Holland). The density of the sintered samples was measured according to the Archimedes method. FTIR spectroscopy of the test materials was carried out by a Fourier transform infrared spectrometer (Bruker, V33 spectrophotometer) from 400 to 4000 cm^{-1}, using KBr pellets containing 1% weight sample in KBr. Also, the surface area (BET) was determined by nitrogen adsorption at −196 °C using an automated gas adsorption analyzer (Micrometrics, Gemini 2375). The BET surface area was used to calculate the mean particle size [D] (Eq. (1)).

$$D = 6/s\rho \quad (1)$$

where 's' is the BET surface area (m^2/g) and 'ρ' is the density of forsterite (kg/m^3). The density of forsterite was considered as 3.27×10^3 (kg/m^3).

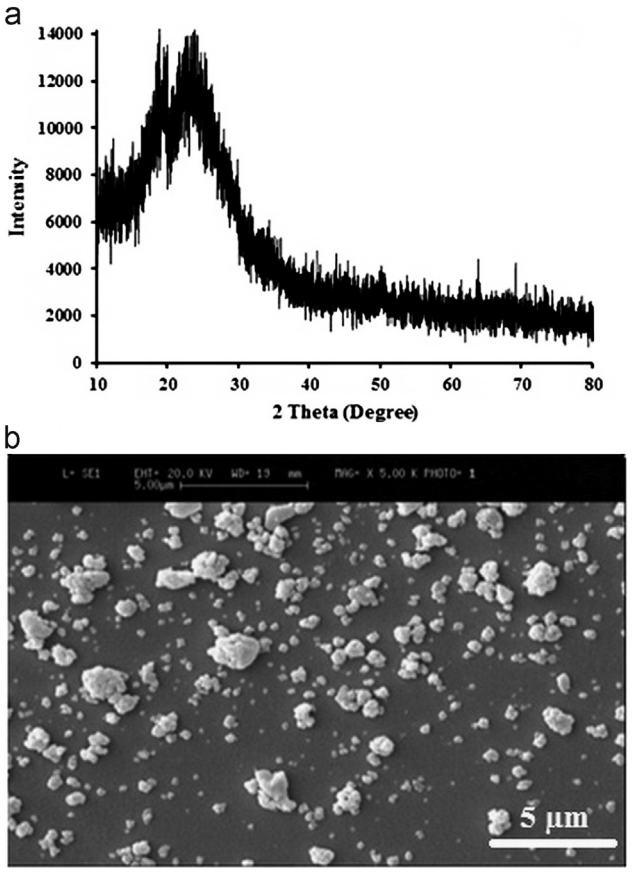

Fig. 2. (a) XRD and (b) SEM silica gel powder before high energy ball milling.

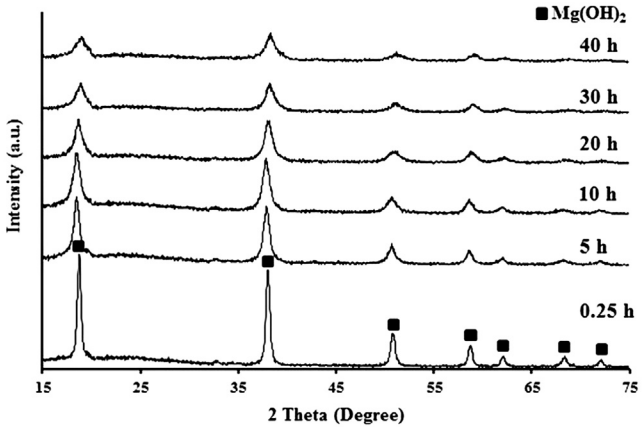

Fig. 3. The XRD patterns of the mixture of initial precursor at various ball-milling times.

3. Results and discussion

Fig. 3 shows the XRD patterns of the mixtures after various milling times at room temperature. The XRD patterns of initial powders after 0.25 h of high energy milling corresponded to those of $Mg(OH)_2$ phases. Increasing the milling time to 40 h was observed to result in the broadening of XRD peaks as well as a significant decrease in their intensity as a consequence of refinement of crystallite size and the enhancement of the lattice strain. Once crystalline phase was observed in the XRD patterns. Subsequent thermal treatment is necessary to synthesize the forsterite structure. Fig. 4 shows the diffraction patterns of the powders milled for 40 h after several thermal treatments at temperatures between 500 and 1200 °C. At the lowest tested temperature (500 °C), a forsterite-structured material was crystallized. As the calcination temperature increased up to 900 °C, pure forsterite was obtained. However, the calcination at high temperatures resulted in an increase in peak intensity which is ascribed to the enhancement of crystallite size. Hence, XRD provides some valuable evidence that the pure forsterite phase can be obtained by high-energy ball milling of powders calcined at 900 °C using microwave processing. In this case, the calcination temperature decreases to 100 °C as compared to conventional solid state reaction of a high-energy ball milled powder [20]. Therefore, the calcination temperature of forsterite was determined to be 900 °C. Observations via scanning electron microscopy revealed that the milling process strongly affects the particle morphology and size. Fig. 5 shows the SEM micrographs of the powders milled for different times. During the milling, the particles are constantly impacted and fractured leading to a considerable reduction of the particle size as a result of the energy provided during the ball milling. Initially, they formed larger aggregates, then broken up in further steps of the milling process. Consequently, uniform grain size distribution is observed with the increase of milling time. It can be seen that the milled powders after 0.25 and 5 h contain larger particles and agglomerates but with the increase of milling time up to 20 h, the particles and agglomerates size will decrease. However, with further increase of the milling time, the microstructure becomes finer and more homogenous. Fig. 6 presents the SEM images of the powder high energy ball milled for 40 h and heat treated at different temperatures. After heat treatment at 500 °C, no particle coarsening occurred and the shape and size remained almost the same as those of milled powder. It can be seen that the particle sizes lightly increased as a function of calcination temperature and this is in good agreement with the particle size estimated using the BET method. The TEM micrograph of the single-phase forsterite nanopowder obtained from 40 h high energy ball milling with

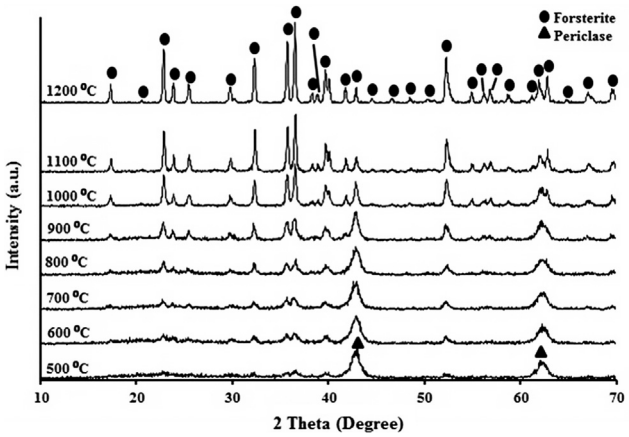

Fig. 4. XRD patterns of the mixtures initial precursors milled for 40 h and calcined at different temperatures by microwave heating.

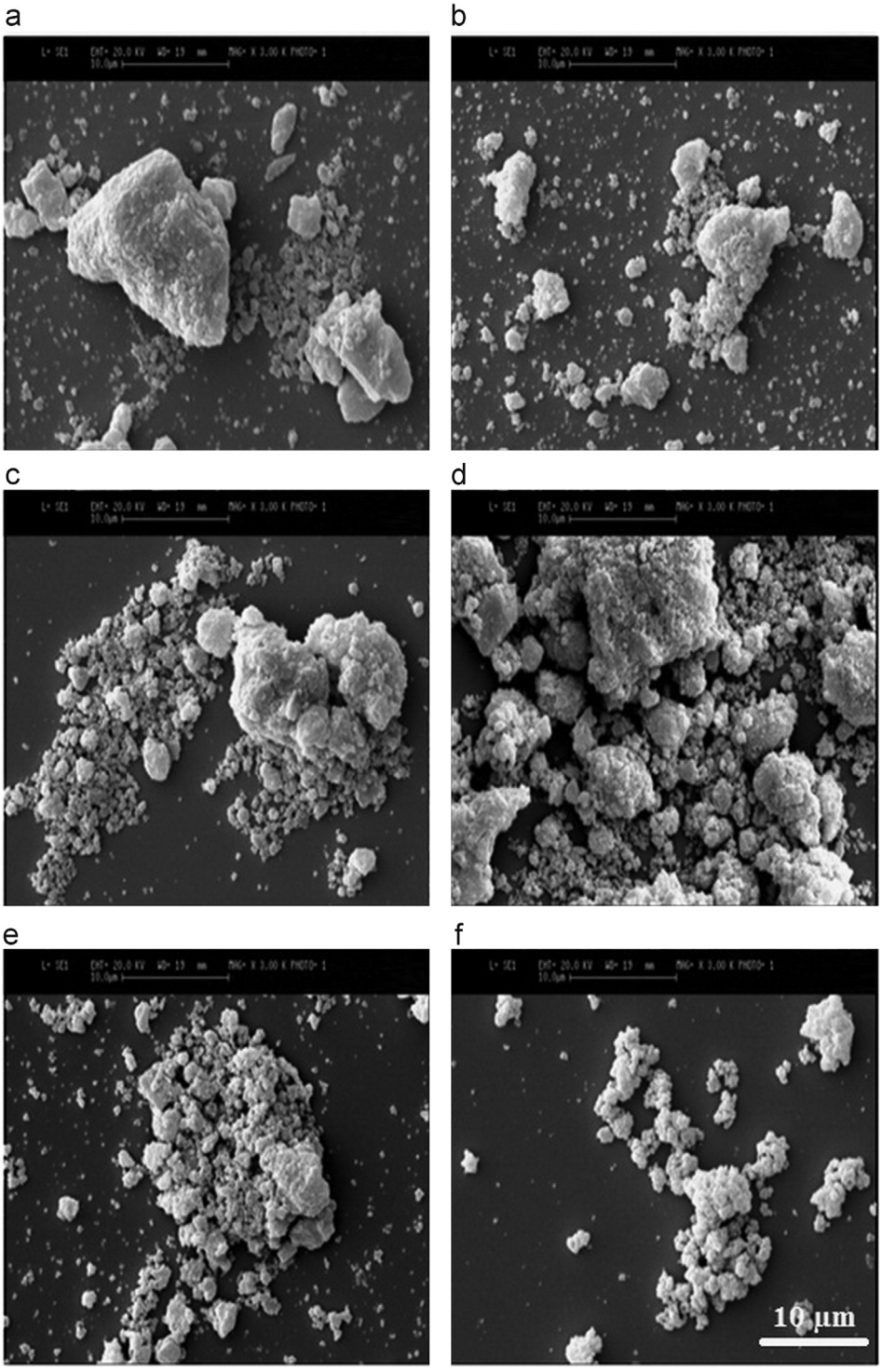

Fig. 5. SEM micrograph of the mixture of the initial precursors milled for different times, (a) 0.25 h, (b) 5 h, (c) 10 h, (d) 20 h, (e) 30 h and (f) 40 h.

subsequent calcination at 900 °C by microwave heating is shown in Fig. 7. It is clear that the average particle diameter of product was less than 100 nm. Based on the results obtained by TEM investigations, it may be concluded that high energy ball milling with subsequent calcination can be useful for synthesizing the forsterite nanopowder. The infrared spectra of the ball milled and synthesized forsterite powders in the 4000–400 cm^{-1} range are shown in Fig. 8. For the mixture of initial precursors milled for 0.25 h, the observed bonds in the FT-IR spectrum corresponded to silica gel and magnesium hydroxide. As the FTIR spectra shown in Fig. 8, the sharp and intense peak at 3697 cm^{-1} was due to the OH group in magnesium hydroxide, the strong peak at around 440 cm^{-1} was assigned to the Mg–O stretching vibration [31,32]. The intense bands related to the siloxane stretching (Si–O–Si) of these groups at 470, 800, and 1090 cm^{-1} are ascribed to the bending modes,

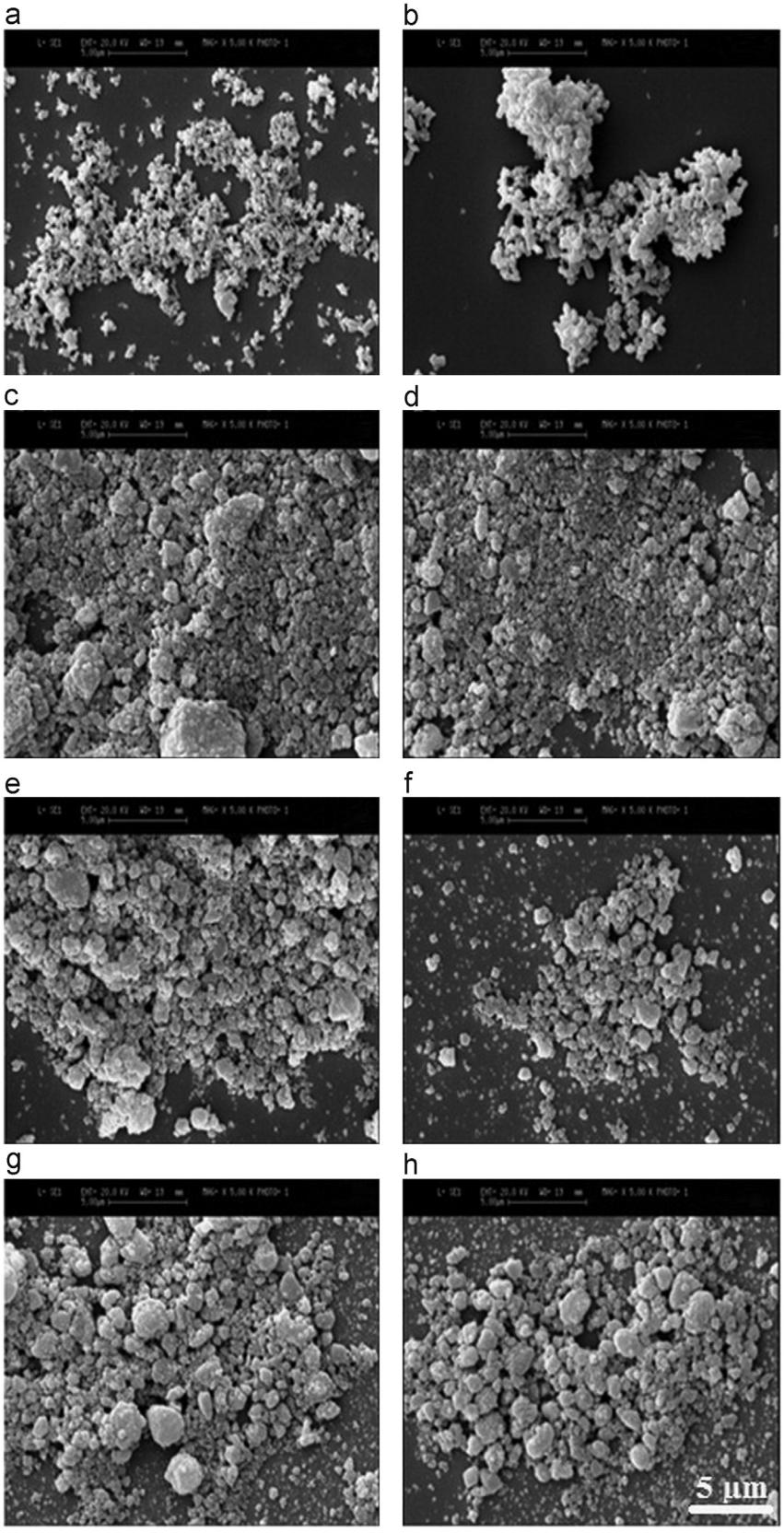

Fig. 6. SEM micrograph of the mixtures initial precursors milled for 40 h and calcined at (a) 500 °C, (b) 600 °C, (c) 700 °C, (d) 800 °C, (e) 900 °C, (f) 1000 °C, (g) 1100 °C and (h) 1200 °C, by microwave heating.

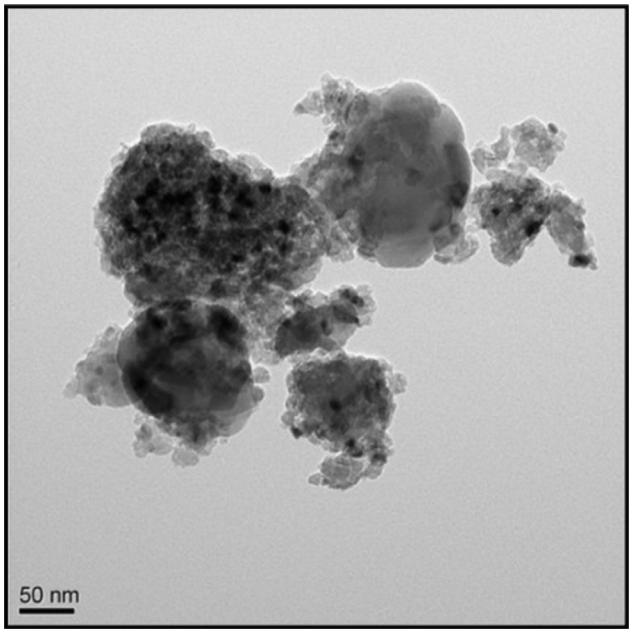

Fig. 7. TEM of the mixture of initial precursors milled for 40 h and calcined at 900 °C by microwave heating.

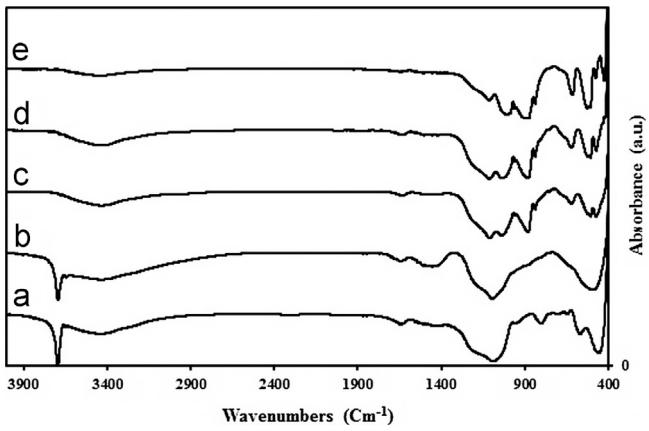

Fig. 8. FTIR spectra of ball milled mixture of initial precursors at (a) 0.25 h, (b) 40 h and the calcined powders at (c) 600 °C, (d) 800 °C and (e) 1000 °C.

symmetric vibration and asymmetric stretching of the Si–O–Si, respectively [33]. With increasing milling time to 40 h, the intensity of bonds related to the mixture of initial precursors decreased and these bonds were observed to broaden. The infrared spectra of forsterite powder obtained after 40 h milling and subsequent annealing at different temperature is illustrated in Fig. 8c–e. The spectra clearly display the peaks of Si–O bands in the SiO_4 tetrahedron that prove the formation of forsterite as it is shown in the XRD pattern of this sample. The bands related to the characteristic peaks of forsterite appear at 1007, 986, 960, 873, and 838 cm^{-1} (SiO_4 stretching), at 616, 527, and 507 cm^{-1} (SiO_4 bending), and at 475 cm^{-1} for modes of octahedral MgO_6. Band positions for the prepared forsterite agreed with the results reported in previous studies [2,20]. The effect of calcination temperature on the surface area and particle size is shown in Table 1. The surface area increases at 900 °C ($\approx$ 40.1 m^2/g); while decreases at higher

Table 1
Surface area, particle size and crystallite size of spinel nanopowders at different temperatures.

Sample	Surface area ($m^2\ g^{-1}$)	Particle size (nm)
Ball milled for 40 h	30.7	–
Calcined at 900 °C	40.1	45
Calcined at 1000 °C	38.8	47
Calcined at 1100 °C	34.3	53
Calcined at 1200 °C	27.5	64.5

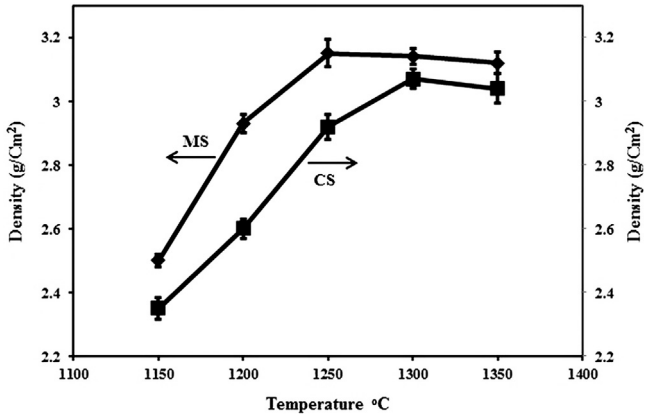

Fig. 9. Relative density of forsterite ceramics prepared using conventional and microwave sintering techniques.

temperatures. Increasing the surface area of the mixture of initial precursors is due to the rapid decomposition accompanied by the appearance of considerable stresses, which leads to decomposition of the particles. With increasing temperature from 900 to 1200 °C, the surface area decreases as the particle size increases due to the grain growth. By increasing the temperature above 1000 °C, the surface diffusion can be activated and caused sintering by formation of necks between particles. Therefore, the surface area reduces as the particle size increases with a higher rate above 1000 °C. Nanocrystalline forsterite powder was sintered at different temperatures using conventional and microwave sintering techniques, and the relative densities obtained are shown in Fig. 9. It can be seen that the relative density of the conventional sintered samples has improved by increasing the sintering temperature, merely reaching 93.7% of the theoretical value at 1300 °C for 120 min. The variation of the relative density of the microwave-sintered samples is similar to that of the conventional-sintered sample. However, its relative density reaches up to 96.2% of the theoretical value at 1250 °C without soaking time. Fig. 10 shows SEM images of the fracture surface of forsterite prepared using conventional and microwave sintering techniques. It can be seen that there is a marked difference between fracture surfaces of the forsterite samples. In Fig. 10(a), it can be seen that the foraterite ceramics produced by conventional processing are rather porous; thus, the densification of the ceramic is insufficient. For microwave processing, the densification in the sintered specimen is enhanced considerably, as shown in Fig. 10(b).

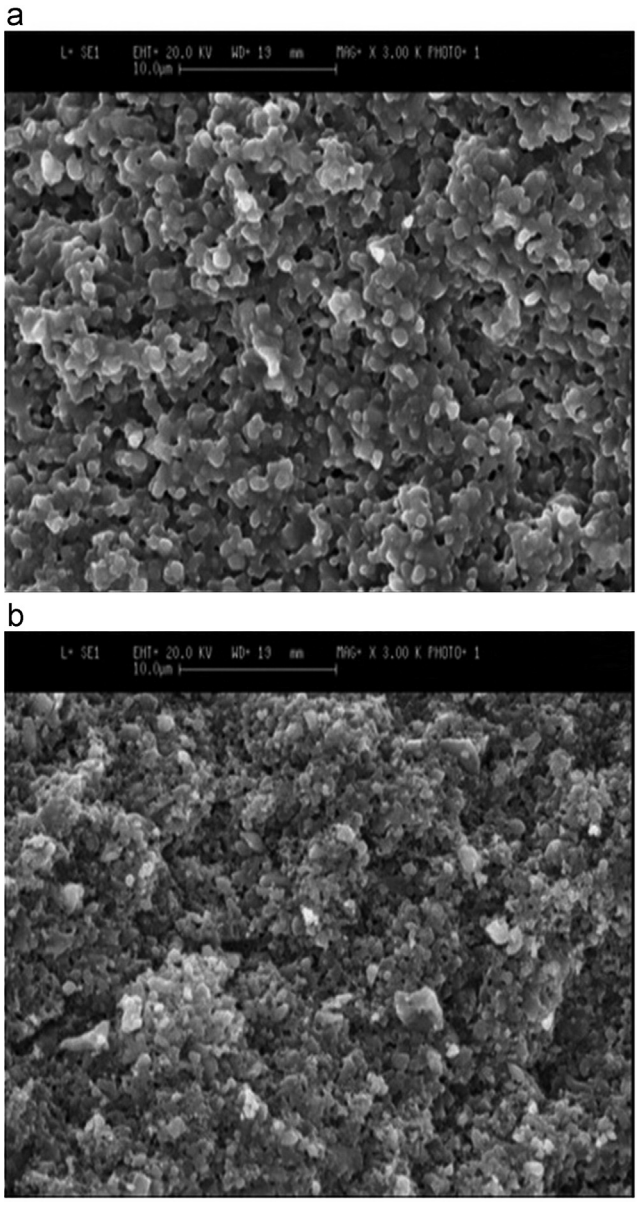

Fig. 10. SEM images of fracture surface of the forsterite at (a) 1200 °C for 120 min using conventional sintering, and at (b) 1250 °C without soaking time.

Also, compared with CS samples, MS samples show smaller grain size as shown in SEM images.

4. Conclusions

In this paper, the microwave assisted high-energy ball milling technique was used to prepare nanosized forsterite (Mg_2SiO_4). The results showed that the single-phase forsterite was formed at the relatively low temperature of about 900 °C without unreacted SiO_2 and MgO phases. Powders with nanosized microstructures were formed. Moreover, BET results determined that the particle sizes of synthesized powders lie in the range of 45–64.5 nm, respectively. From the study of forsterite ceramics prepared by microwave sintering and conventional sintering, it is seen that MS samples possessed smaller grain size, better densification and more uniform grain growth.

Reference

[1] C. Suryanarayana, Mechanical alloying and milling, Prog. Mater. Sci. 46 (2001) 1–184.
[2] C. Kosanovic, N. Stubicar, N. Tomasic, V. Bermanec, M. Stubicar, Synthesis of a forsterite powder by combined ball milling and thermal treatment, J. Alloys Compd. 389 (2005) 306–309.
[3] S.A. Boppart, G.J. Tearney, B.E. Bouma, J.F. Southern, M.E. Brezinski, J.G. Fujimoto, Noninvasive assessment of the developing Xenopus cardiovascular system using optical coherence tomography, Proc. Natl. Acad. Sci. USA 94 (1997) 4256–4261.
[4] B.R. Washburn, S.A. Diddams, N.R. Newbury, J.W. Nicholson, M.F. Yan, C.G. Jorgensen, Phaselocked erbium-fiber-laser-based frequency comb in the near infrared, Opt. Lett. 29 (2004) 250–252.
[5] L. Lin, M. Yin, C. Shi, W. Zhang, Luminescence properties of a new red long-lasting phosphor: $Mg_2SiO_4:Dy^{3+}$, Mn^{2+}, J. Alloys Compd. 455 (2008) 327–330.
[6] G.W. Brindley, R. Hayami, Kinetics and mechanism of formation of forsterite (Mg_2SiO_4) by solid state reaction of MgO and SiO_2, Philos. Mag. Lett. 12 (1965) 505–514.
[7] A. Douy, Aqueous synthesis of forsterite (Mg_2SiO_4) and enstatite ($MgSiO_3$), J. Sol–Gel Sci. Technol. 24 (2002) 221–228.
[8] A.G.M. Othman, N.M. Khalil, Sintering of magnesia refractories through the formation of periclase–forsterite-spinel phases, Ceram. Int. 31 (2005) 1117–1121.
[9] V. Petricevic, S.K. Gayen, R. Alfano, K. Yamagishi, Laser action in chromium-doped forsterite, Appl. Phys. Lett. 52 (1988) 1040–1043.
[10] F. Tavangarian, R. Emadi, Effects of mechanical activation and chlorine ion on nanoparticle forsterite formation, Mater. Lett. 65 (2011) 126–129.
[11] L. Cheng, P. Liu, X.M. Chen, W.C. Niu, G.G. Yao, C. Liu, X.G. Zhao, Q. Liu, H.W. Zhang, Fabrication of nanopowders by high energy ball milling and low temperature sintering of Mg_2SiO_4 microwave dielectrics, J. Alloys Compd. 513 (2012) 373–377.
[12] F. Tavangarian, R. Emadi, Nanostructure effects on the bioactivity of forsterite bioceramic, Mater. Lett. 65 (2011) 740–743.
[13] H. Ghomi, M. Jaberzadeh, M.H. Fathi, Novel fabrication of forsterite scaffold with improved mechanical properties, J. Alloys Compd. 509 (2012) L63–L68.
[14] M.H. Fathi, M. Kharaziha, Two-step sintering of dense, nanostructural forsterite, Mater. Lett. 63 (2009) 1455–1458.
[15] M.T. Tsai, Hydrolysis and condensation of forsterite precursor alkoxides: modification of the molecular gel structure by acetic acid, J. Non-Cryst. Solids 298 (2002) 116–130.
[16] M.H.E. Martin, C.K. Ober, C.R. Hubbard, W.D. Porter, O.B. Cavin, Poly (methacrylate) precursors to forsterite, J. Am. Ceram. Soc. 75 (1992) 1831–1838.
[17] A. Saberi, Z. Negahdari, B. Alinejad, F. Golestani-Fard, Synthesis and characterization of nanocrystalline forsterite through citrate–nitrate route, Ceram. Int. 35 (2009) 1705–1708.
[18] A. Kazakos, S. Komarneri, R. Roy, Preparation and densification of forsterite (Mg_2SiO_4) by nanocomposite sol–gel processing, Mater. Lett. 9 (1990) 405–409.
[19] D.G. Park, J.C. Duchamp, T.M. Duncan, J.M. Burlitch, Preparation of forsterite by pyrolysis of a xerogel: the effect of water, Chem. Mater. 6 (1994) 1990–1995.
[20] K.P. Sanosh, A. Balakrishnan, L. Francis, T.N. Kim, Sol–gel synthesis of forsterite nanopowders with narrow particle size distribution, J. Alloys Compd. 495 (2010) 113–115.
[21] K. Mostafavi, M. Ghahari, S. Baghshahi, A.M. Arabi, Synthesis of $Mg_2SiO_4:Eu^{3+}$ by combustion method and investigating its luminescence properties, J. Alloys Compd. 555 (2013) 62–67.
[22] F. Tavangarian, R. Emadi, A. Shafyei, Influence of mechanical activation and thermal treatment time on nanoparticle forsterite formation mechanism, Powder Technol. 198 (2010) 412–416.

[23] F. Tavangarian, R. Emadi, Synthesis of nanocrystalline forsterite (Mg_2SiO_4) powder by combined mechanical activation and thermal treatment, Mater. Res. Bull. 45 (2010) 388–391.
[24] F. Tavangarian, R. Emadi, A. Shafyei, Influence of mechanical activation and thermal treatment time on nanoparticle forsterite formation mechanism, Powder Technol. 198 (2010) 412–416.
[25] D. Mingos, P. Michael, Microwave syntheses of inorganic materials, Adv. Mater. 5 (1993) 857–859.
[26] T. Ebadzadeh, M.H. Sarrafi, E. Salahi, Microwave-assisted synthesis and sintering of mullite, Ceram. Int. 35 (2009) 3175–3179.
[27] T. Ebadzadeh, Formation of mullite from precursor powders: sintering, microstructure and mechanical properties, Mater. Sci. Eng. A355 (2003) 56–61.
[28] S. Barison, M. Fabrizio, S. Fasolin, F. Montagner, C. Mortalo, A microwave-assisted sol–gel Pechini method for the synthesis of $BaCe_{0.65}Zr_{0.20}Y_{0.15}O_3$-d powders, Mater. Res. Bull. 45 (2010) 1171–1176.
[29] H. Mohebbi, T. Ebadzadeh, F.A. Hesari, Synthesis of nano-crystalline NiO–YSZ by microwave-assisted combustion synthesis, Powder Technol. 188 (2009) 183–186.
[30] N Shojaee, T Ebadzadeh, A Aghaei, Effect of concentration and heating conditions onmicrowave-assisted hydrothermal synthesis of ZnO nanorods 61 (2010) 1418–1423Mater. Charact. 61 (2010) 1418–1423.
[31] W. Jiang, X. Hua, Q. Han, X. Yang, L. Lu, X. Wang, Preparation of lamellar magnesium hydroxide nanoparticles via precipitation method, Powder Technol. 191 (2009) 227–230.
[32] D. An, X. Ding, Z. Wang, Y. Liu, Synthesis of ordered arrays of magnesium hydroxide nanoparticles via a simple method, Colloid Surf. A: Physicochem. Eng. Asp. 356 (2010) 28–31.
[33] N. Pijarn, A. Jaroenworaluck, W. Sunsaneeyametha, R. Stevens, Synthesis and characterization of nanosized-silica gels formed under controlled conditions, Powder Technol. 203 (2010) 462–468.